Lab Notes

Editors
Thomas M. Moses | Shane F. McClure | Sally Eaton-Magaña

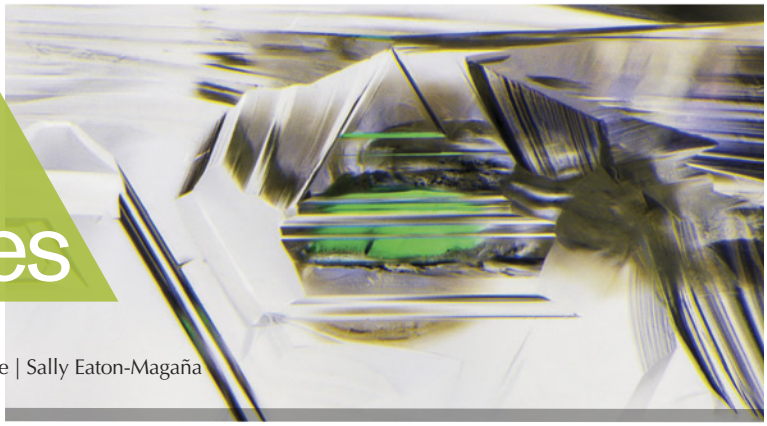

DIAMOND

Rare Natural Bicolor Diamond

A 0.63 ct bicolor diamond was submitted to GIA at the 2023 Tucson gem show for scientific examination. Previously submitted to GIA in 2008 for a colored diamond grading report, this tapered baguette-cut natural diamond had two major color zones: Fancy Dark orangy brown and Fancy Dark brown greenish yellow (figure 1). The brown greenish yellow zone had chameleon properties, including a temporary color change upon heating or when left in darkness for an extended period of time (possibly days). Visible narrow bands with darker color were observed within the brown greenish yellow zone (figure 1). Fourier-transform infrared spectra collected from the two color zones indicated that both were type Ia with comparable nitrogen concentrations. No amber centers or carbon dioxide absorption were detected in either color zone.

Bicolor diamonds are very uncommon, and the colors likely result from a combination of lattice defects. The major causes for yellow coloration in diamond include N3 centers, C centers, H3 centers, and the 480 nm absorption band (C.M. Breeding et al., "Naturally colored yellow and orange gem diamonds: The nitrogen factor," Summer 2020 *G&G*, pp. 194–219), whereas brown coloration is typically associated with vacancy clusters produced during plastic deformation (D. Fisher, "Brown diamonds and high pressure high temperature treatment," *Lithos*, Vol. 112, Supplement 2, 2009, pp. 619–624). It has been reported that diamonds rich in carbon dioxide might also have a brown color (T. Hainschwang et al., "HPHT treatment of CO_2 containing and CO_2-related brown diamonds," *Diamond and Related Materials*, Vol. 17, 2008, pp. 340–351). Ultraviolet/visible/near-infrared spectra collected separately from the two color zones to determine their color origins indicated that both color zones contained the 480 nm absorption band. In addition to this 480 nm absorption band, the brown color zone also showed enhanced absorption extending from the near-infrared region toward the UV region of the spectrum.

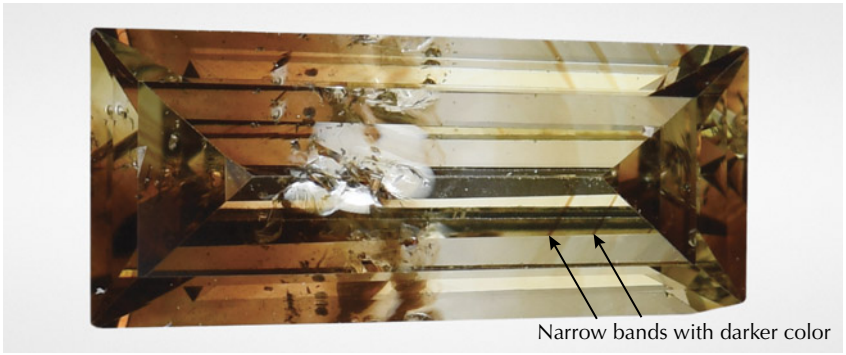

Figure 1. This 0.63 ct tapered baguette-cut diamond showed two major color zones.

Diamonds colored by the 480 nm absorption band generally have multiple growth zones with distinct fluorescence colors excited by deep UV (<230 nm), due to their complex multi-stage growth under changing conditions in the earth's mantle (Breeding et al., 2020). This bicolor diamond had alternating blue and greenish yellow fluorescence zones (figure 2), similar to the fluorescence patterns in other diamonds with the 480 nm absorption band. The fluorescence zones did not correlate with the major color zoning (i.e., orangy brown and brown greenish yellow) in this diamond. However, the greenish yellow fluorescence bands (figure 2) appeared to correspond to the narrow bands with darker color in the brown greenish yellow color zone (figure 1).

A cluster of orange mineral inclusions was observed beneath the table facet, where the largest inclusion measured 180 µm in maximum dimension (figure 3). The Raman spectrum of the largest inclusion showed the characteristic peaks of pyrope-almandine-grossular garnet, $(Mg,Fe,Ca)_3Al_2(SiO_4)_3$, at

Editors' note: All items were written by staff members of GIA laboratories.

Gems & Gemology, Vol. 59, No. 4, pp. 486–498.

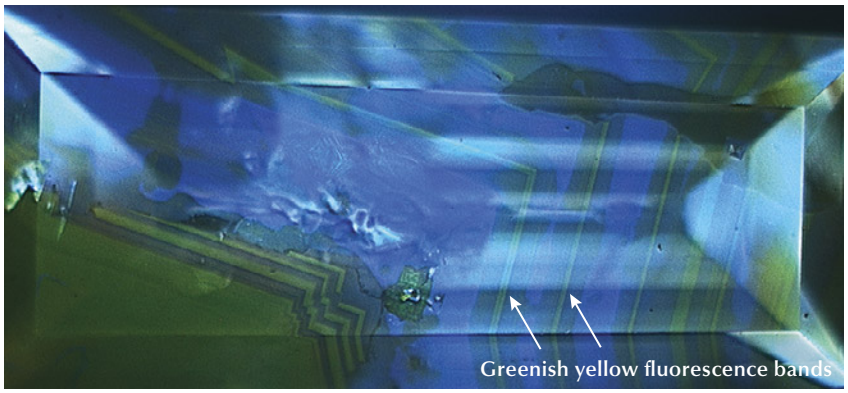

Figure 2. Alternating blue and greenish yellow fluorescence zones were observed with deep-UV excitation. This fluorescence pattern is typical for diamonds colored by the 480 nm visible absorption band.

358, 558, and 917 cm^{-1} (e.g., E.M. Smith et al., "Raman identification of inclusions in diamond," *Reviews in Mineralogy and Geochemistry*, Vol. 88, 2022, pp. 451–473), indicating the diamond was associated with eclogite host rocks having pyrope-almandine-grossular garnet as a major constituent mineral.

This unique bicolor diamond exhibiting two distinctly different colors demonstrates the variety possible within the natural world.

Mei Yan Lai and Sally Eaton-Magaña

Carbon Dioxide in a Brown Diamond

The Carlsbad laboratory recently examined a 1.03 ct natural Fancy Dark brown diamond with uneven color zoning and abundant black inclusions (figure 4). The diamond had infrared absorption features at 2370 and 659 cm^{-1}, corresponding to the asymmetric stretching mode and bending mode of carbon dioxide, respectively (E. Barannik et al., "Shift of CO_2-I absorption bands in diamond: A pressure or compositional effect? A FTIR mapping study," *Diamond and Related Materials*, Vol. 113, 2021, article no. 108280). Diamonds containing carbon dioxide are rarely submitted for diamond grading reports, and this brown diamond is one of the few GIA has encountered. Carbon dioxide likely exists as submicroscopic solid inclusions in natural diamond (M. Schrauder and O. Navon, "Solid carbon dioxide in a natural diamond," *Nature*, Vol. 365, 1993, pp. 42–44). The major infrared absorption peaks observed are shifted from the peak positions of atmospheric carbon dioxide (2350 and 667 cm^{-1}), and the peak shift depends on pressure and the presence of impurities such as water and nitrogen in the trapped carbon dioxide inclusions (Barannik et al., 2021).

Carbonate-related absorptions at 1433 and 870 cm^{-1} were also detected. These absorptions have previously been reported in some natural diamonds containing solid carbon dioxide inclusions (e.g., Summer 2005 Lab Notes, pp. 165–167; Barannik et al., 2021). Clusters of black hexagonal inclusions were observed in the diamond

Figure 3. Multiple orange inclusions were observed in this bicolor diamond. The largest was identified as pyrope-almandine-grossular garnet. Field of view 1.76 mm.

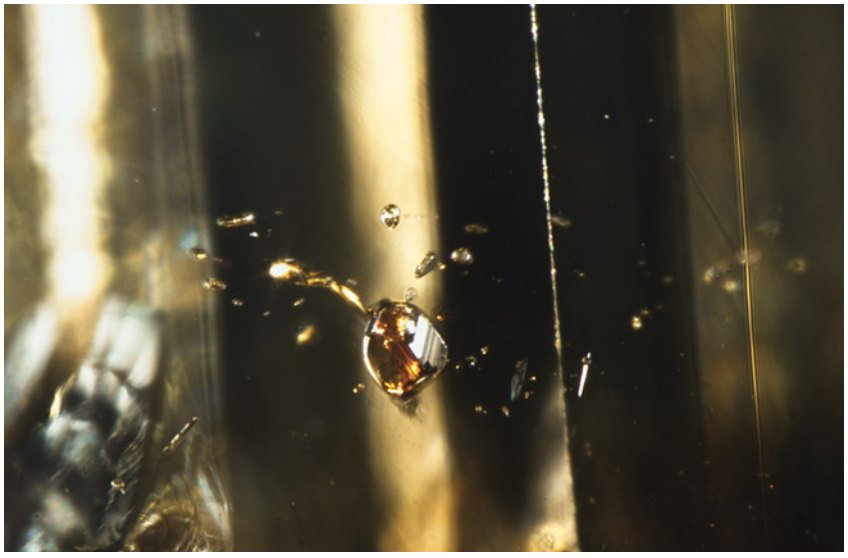

Figure 4. This 1.03 ct natural Fancy Dark brown diamond has uneven color zoning and abundant black inclusions. Infrared absorptions corresponding to carbon dioxide (2370 and 659 cm^{-1}) and carbonate (1433 and 870 cm^{-1}) were detected.

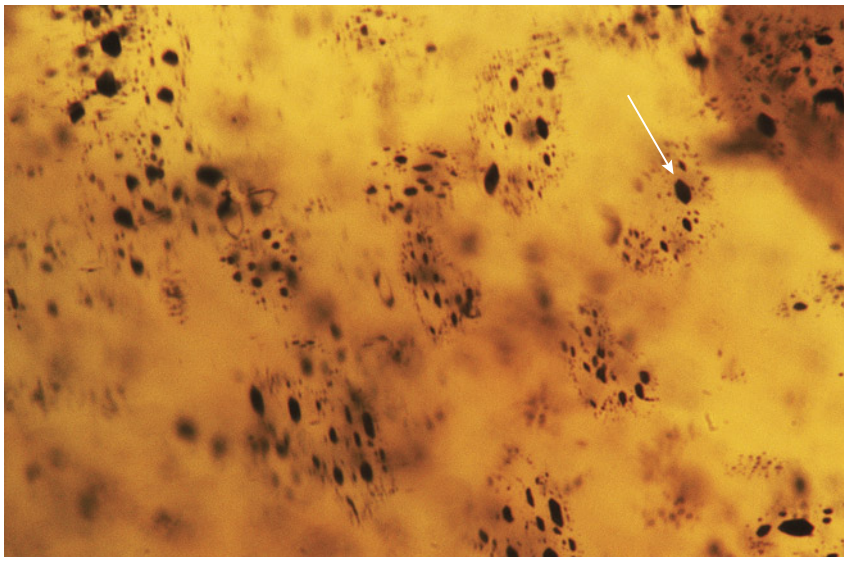

Figure 5. Microscopic examination under high magnification revealed the hexagonal shape of the black inclusions. Field of view 1.26 mm.

(figure 5), and the individual inclusions ranged in size from <1 to ~50 µm. Similar inclusions have been documented in some carbon dioxide–bearing natural diamonds and identified as graphite platelets (A. Shiryaev et al., "Exsolution of oxygen impurity from diamond lattice and formation of pressurized CO_2-I precipitates," *Carbon Trends*, Vol. 11, 2023, article no. 100270).

This brown diamond containing carbon dioxide displayed yellow fluorescence when exposed to long-wave UV. When exposed to deep UV (<230 nm), the diamond exhibited irregular surface fluorescence zoning with yellowish green, bright green, and blue colors caused by distinct lattice defects. The yellow fluorescence to long-wave UV, heterogeneous distribution of lattice defects, and irregular surface fluorescence zoning under deep-UV excitation are commonly observed in diamonds colored by the 480 nm absorption band (known as "480 nm band diamonds" in the trade; C.M. Breeding et al., "Naturally colored yellow and orange gem diamonds: The nitrogen factor," Summer 2020 *G&G*, pp. 194–219). In fact, the photoluminescence (PL) spectra of this brown diamond closely resembled those of 480 nm band diamonds. The most notable PL feature detected was the broad band centered at ~680 nm, which is attributed to the vibronic emission associated with the 480 nm absorption band (A. Collins and K. Mohammed, "Optical studies of vibronic bands in yellow luminescing natural diamonds," *Journal of Physics C: Solid State Physics*, Vol. 15, 1982, pp. 147–158). The similarity in spectroscopic features between carbon dioxide–bearing brown diamonds and 480 nm band diamonds has been previously reported, and a genetic relationship between the two has been suggested (T. Hainschwang et al., "HPHT treatment of CO_2 containing and CO_2-related brown diamonds," *Diamond and Related Materials*, Vol. 17, 2008, pp. 340–351).

Mei Yan Lai and Virginia Schwartz

Cricket Bat Diamond

As early as the seventeenth century, the British introduced the sport of cricket to the Indian subcontinent, where it is now the most popular sport. Recently, a diamond shaped like a cricket bat (figure 6) was submitted to GIA's Mumbai laboratory for testing. In cricket, a bat is a wooden piece of equipment with a long handle attached to a flat-fronted blade, used to hit the ball. This diamond weighed 1.04 ct and measured 14.20 × 4.12 × 2.13 mm. It had a Light brown color. The bat-shaped diamond was partially polished with a rough texture retained on the tip of the handle and the front part of the bat. According to the diamond manufacturer, the original rough skin is intentionally kept in a few parts to authenticate its natural origin.

Based on spectroscopic features, it was confirmed to be type IIa with a very weak peak at 3107 cm^{-1} (hydrogen-related infrared absorption peak). Photoluminescence spectra collected at liquid nitrogen temperature with varying laser excitations revealed its natural origin; no color treatment was detected. A crosshatched "tatami" strain pattern was clearly observed between crossed polarizers when viewed under a microscope.

In photoluminescence spectra collected at room temperature with 405 nm excitation, this diamond also showed the presence of N3, a defect wherein a vacancy is surrounded by three nitrogen atoms.

Figure 6. A 1.04 ct diamond in the shape of a cricket bat, measuring 14.20 mm long.

Figure 7. The cricketer's name and signature inscribed on the diamond.

As shown in figure 7, this special diamond is inscribed with the name and signature of Virat Kohli, who is widely regarded as one of the greatest players in the history of the sport. The owner of the diamond intends to gift it to Kohli.

Manisha Bhoir, Shoko Odake, and Wuyi Wang

Treated HPHT LABORATORY-GROWN DIAMOND with Dramatic Color Zoning

Recently, the Carlsbad laboratory examined a 2.20 ct laboratory-grown diamond that received a color grade of Fancy Deep brownish orange (figure 8). Spectroscopic analysis indicated high-pressure, high-temperature (HPHT) growth methods and subsequent irradiation and annealing to create nitrogen vacancy centers. Infrared absorption spectra collected from the entire stone identified it as type Ib with a concentration of ~5 ppm of single isolated nitrogen. The diamond was distinctive because of a pronounced pink square under the table facet within the cubic {100} sector. The other major growth sectors (e.g., {110}, {111}) surrounding the central cubic sector appeared yellow due to single isolated nitrogen. The pink growth sector displayed pronounced reflections when viewed through the pavilion facets and had more of a purple color (figure 9).

Figure 8. This 2.20 ct Fancy Deep brownish orange treated HPHT-grown diamond owes its distinctive appearance to multiple defect concentrations created within the various growth sectors.

Visible/near-infrared (Vis-NIR) absorption spectra were collected from the center of the table using a reflectance probe positioned to show pink fluorescence. The probe was then repositioned toward the crown facets that did not show pink fluorescence (figure 10). The spectra from both areas indicated type Ib-related absorption at low wavelengths. Additionally, the pink color region was dominated by the NV^- center (zero-phonon line, or ZPL, at 637 nm) and its associated sidebands, while the surrounding yellow regions had minor absorption from NV^0 (ZPL at 575 nm). This difference in NV-related absorption shifts the transmission window from pink to yellow.

The uptake of single nitrogen is generally lower in {100} growth sectors than in {111} sectors (R.C. Burns et al., "Growth-sector dependence of optical features in large synthetic diamonds," *Journal of Crystal Growth*, Vol. 104, 1990, pp. 257–279). However, the concentration of single nitrogen (necessary to ultimately create NV centers) can be increased within the cubic sector through lower growth temperatures (S. Satoh et al., "Differences in nitrogen concentration and aggregation among {111} and {100} growth sectors of large synthetic diamonds," *Science and Technology of New Diamond*, KTK Scientific Publishers/Terra Scientific Publishing Co., Tokyo, 1990, pp. 351–355). It is possible that such growth conditions were used with this diamond in order to incorporate sufficient nitrogen within the cubic sectors, which were subsequently transformed to NV centers with treatment.

Within the cubic sector, photoluminescence (PL) mapping showed a significantly higher concentration of NV^- compared with the other major growth sectors (e.g., {110} and {111}), while the concentration of NV^0 was lower (figure 11). The presence of donors, such as single nitrogen, can often shift the balance between neutral and negative NV centers so that NV^- is enhanced in diamonds with single nitrogen (I.A. Dobrinets et al., *HPHT-Treated Diamonds: Diamonds Forever*, 2013,

Figure 9. The square-shaped cubic {100} growth sector appears pink when viewed through the table (left) and more of a purple color when viewed through the pavilion (right). The surrounding regions appear predominantly yellow due to the presence of single nitrogen. Fields of view 4.23 mm and 4.50 mm.

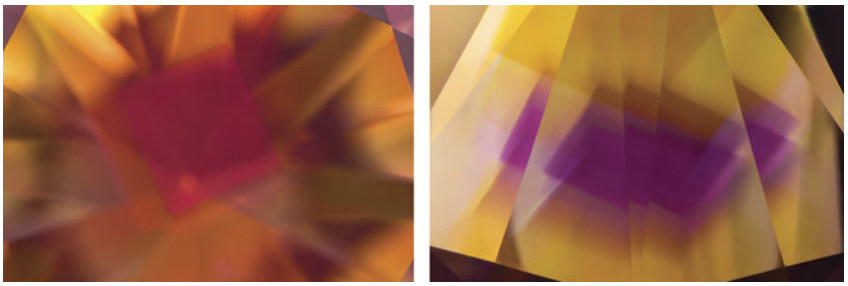

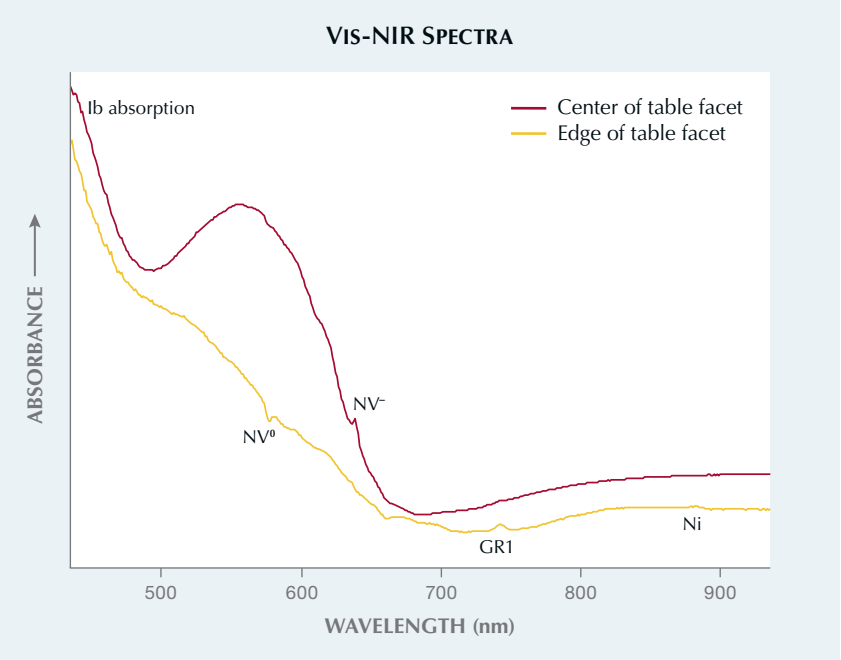

Figure 10. Room-temperature Vis-NIR absorption spectra were collected using a reflectance probe to document the absorption differences between the pink central region and the surrounding areas. The red trace shows a pronounced absorption associated with NV^- along with Ib (i.e., single nitrogen) absorption. The yellow trace also shows Ib absorption along with a minor contribution of NV^0 and small peaks associated with GR1 (741.2 nm) and nickel (883/884 nm). Spectra are offset vertically for clarity.

Springer-Verlag, Berlin). The presence of single nitrogen can be related to an elevated concentration of NV^- within the cubic sector; however, in the {111} sectors, NV^0 dominates over NV^- despite the appreciable concentrations of single nitrogen. This can likely be attributed to the {111} sectors also preferentially incorporating boron. Although boron was not detected within the infrared absorption spectra for this stone, it is often present in HPHT-grown diamond, even at low concentrations. Since boron preferentially incorporates within {111} sectors (U.F.S. D'Haenens-Johansson et al., "Synthesis of diamonds and their identification," *Reviews in Mineralogy and Geochemistry*, Vol. 88, No. 1, 2022, pp. 689–753), these acceptors could shift the charge balance within those areas, thus causing the preferential creation of NV^0 over NV^-.

PL mapping highlighted other pronounced differences between the growth sectors. The GR1 defect (V^0) and TR12, an irradiation-related defect with ZPL at 469.9 nm, was highest in {110} and negligible in {100}. The nickel-related doublet at 883/884 nm was extremely high in {111} and negligible in {110} and {100}.

This HPHT-grown diamond is a notable example of growth techniques and treatment engineering producing a combination of defects that is visually interesting. The faceting approach, in which the pink growth sector was positioned under the table facet, served to enhance the dramatic appearance.

Sally Eaton-Magaña and Taryn Linzmeyer

Figure 11. PL mapping using 532 nm excitation at liquid nitrogen temperature shows pronounced differences in defect concentrations based on growth sector. The NV^- intensity (left, normalized to the diamond Raman line) is highest within {100} and much lower within the other regions. The normalized NV^0 defect intensity (right) was detected throughout the diamond but was noticeably higher within {111} sectors.

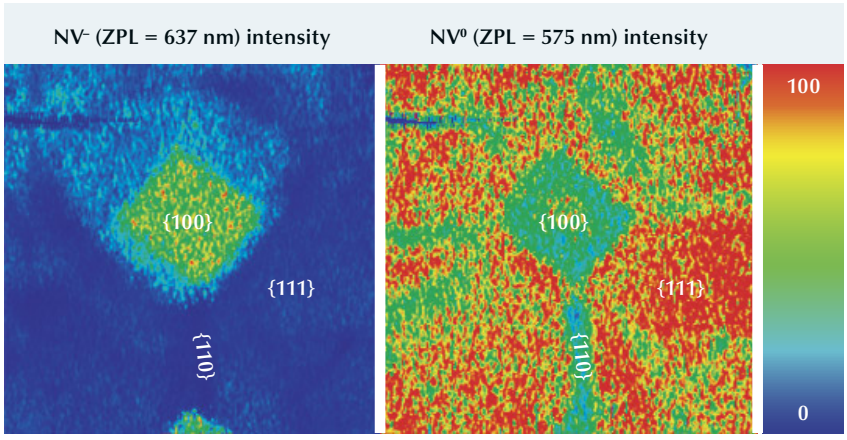

PEARLS

Two Foraminifera-Like Objects Found in a Natural Saltwater Pearl

GIA's Hong Kong laboratory recently received a brown nacreous pearl weighing 1.57 ct and measuring 11.06 × 9.15 × 7.20 mm (figure 12). It had a baroque shape and exhibited a soft luster with an unaltered surface. Despite its size, the pearl felt relatively lightweight, indicating the possibility of a hollow or partially hollow internal structure. Viewed under 40× magnification, the surface displayed overlapping nacre platelets

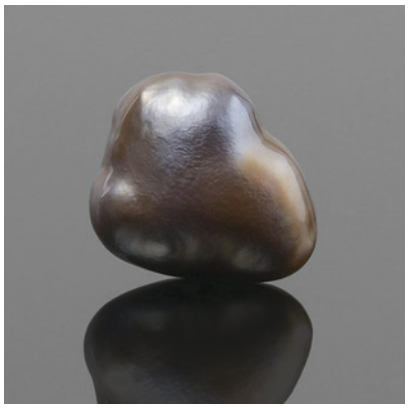

Figure 12. The 1.57 ct brown nacreous pearl measuring 11.06 × 9.15 × 7.20 mm.

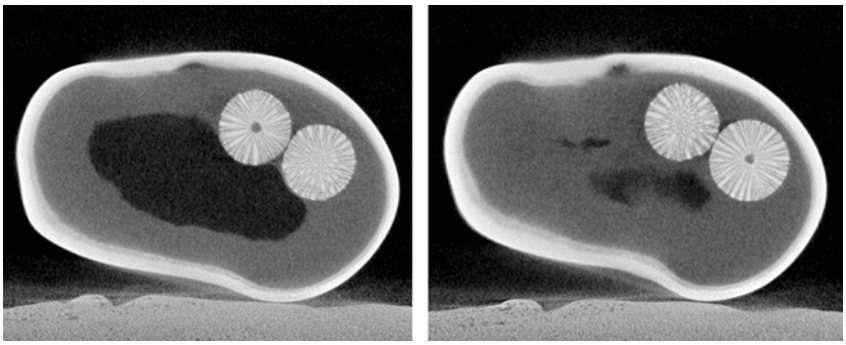

Figure 14. µ-CT images revealed more details of the foraminifera-like spheres. Both consisted of a radiating structure that extended from an empty core.

in a spiral pattern, similar to that observed in pearls produced by *Pteria* species mollusks (L. Kiefert et al., "Cultured pearls from the Gulf of California, Mexico," Spring 2004 *G&G*, pp. 26–39).

The sample exhibited the typical brownish surface tint of pearls produced by the *Pteria* mollusk species. Its ultraviolet/visible spectrum showed the characteristic reflectance features of naturally colored pearls formed in this mollusk, with identifiable absorptions at 405 and 495 nm (S. Karampelas et al., "Spectral differentiation of natural-color saltwater cultured pearls from *Pinctada margaritifera* and *Pteria sterna*," Summer 2011 *G&G*, p. 117). Under long-wave UV radiation, the pearl also displayed moderate red fluorescence, a reaction linked to a type of porphyrin pigment found in pearls originating from the *Pteria* species (Kiefert et al., 2004). Energy-dispersive X-ray fluorescence analysis showed no traces of manganese and 1150 ppm of strontium, confirming its saltwater origin.

Real-time microradiography revealed a fascinating internal structure (figure 13). A large central void, composed of light and dark gray areas associated with the presence of organic matter, occupied almost the entire interior of the pearl, which explained the lighter than expected heft. Surrounding the void, a few distinct growth arcs were observed, following the outline of the pearl's shape—a typical feature seen in natural pearls. In addition, two intriguing foreign materials were trapped within the inner wall of the light gray organic-rich area of the void.

Further analysis via X-ray computed microtomography (µ-CT) imaging revealed the porous nature of these two materials. Resembling foraminifera, a marine micro-skeleton member of a phylum of amoeboid protists, they consisted of radial structures extending from the center of empty cores (figure 14). The pair of near-spherical objects measured 1.50 × 1.25 mm and 1.53 × 1.33 mm, respectively, and appeared to be separate entities while sharing a homogeneous formation. The pearl's structure was judged to be natural due to the appearance of the natural-looking void, which consisted of a flowy outline, and the presence of the foraminifera-like entities. It is worth noting that most cultured pearls from the *Pteria* species available in the market are bead cultured pearls. Non-bead cultured "keshi" *Pteria* pearls are normally of smaller sizes and distinguishable internal structures.

GIA has received numerous pearl submissions in the past with interesting internal structures related to foreign materials. In fact, the skeletal composition of the foreign material observed looked exceedingly similar to that found in a natural pearl examined by GIA's Bangkok laboratory in 2015 (Winter 2015 Lab Notes, pp. 434–435). However, this pearl stands out for the presence of paired foraminifera-like spheres. No two pearls are the same, and it is always rewarding when advanced testing reveals such captivating features.

Cheryl Ying Wai Au

Figure 13. Real-time microradiographs showing the overall internal structure of the pearl (left) and greater detail of the foreign materials (right).

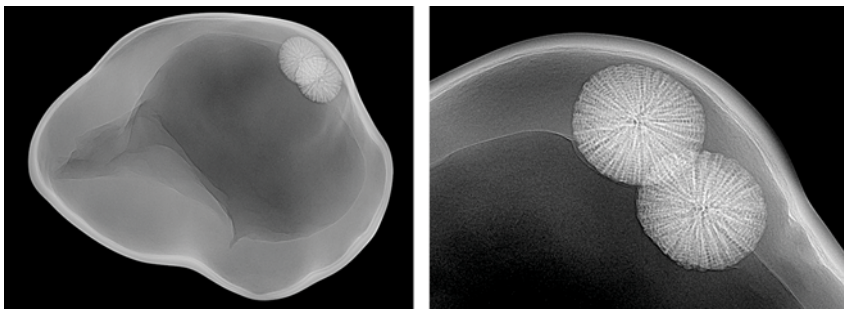

Figure 15. Strands of freshwater bead cultured pearls acquired at the Hong Kong show (top) and freshwater BC pearls submitted for identification (middle) are shown with a strand of 6.60 mm akoya bead cultured pearls (bottom) for comparison.

Small Freshwater Bead Cultured Pearls

Recently, the Carlsbad laboratory received a strand of 78 light bluish gray near-round pearls for identification. The strand (figure 15, middle) weighed 16.75 g (gross), and the pearls measured approximately 5.45 mm in diameter. Upon first impression, they looked like akoya bead cultured (BC) pearls due to their small size and shell bead nuclei observed down the drill holes with a 10× loupe. Their light bluish gray bodycolor also resembled the unprocessed and untreated akoya BC pearls that have become more popular in the market. However, microscopic observation revealed light blue color concentrations under the surface of many pearls (figure 16, left) and blue dye around a surface-reaching feature on one sample (figure 16, right), suggesting that the colors had been artificially modified.

Energy-dispersive X-ray fluorescence chemical analysis showed high levels of manganese, indicating a freshwater origin, as opposed to the saltwater origin of akoya. In 2023, at the AGTA GemFair in Tucson and the Hong Kong International Jewellery show, we saw small near-round to round Chinese freshwater BC pearls around 2–4 mm gaining popularity in the market (Spring 2023 Gem News International, pp. 109–110). These Chinese cultured pearls were available in various colors that were either natural or modified. A strand consisting of 126 small light gray freshwater BC pearls approximately 3.50 mm in diameter (figure 15, top) was acquired at the Hong Kong show to study the internal structures. The light gray bodycolor, likely caused by irradiation considering the dark gray bead nuclei seen in the drill holes, was atypical for natural colored freshwater pearls.

Real-time microradiography (RTX) revealed a distinct bead nucleus in each pearl in both the strand submitted for identification (figure 17, top) and the strand obtained from the Hong Kong show (figure 17, bottom), confirming they were bead cultured. All the pearls displayed relatively thick nacre, averaging about 1 mm for the larger strand and 0.8 mm for the smaller strand. The bead nuclei measured approximately 3.5 mm and 2.7 mm in diameter, respectively.

Although this type of small freshwater BC pearl is generally smaller than typical akoya BC pearls, there are

Figure 16. Left: Multiple blue color concentrations under the surface of one pearl; field of view 19.27 mm. Right: Blue dye concentration inside a fracture; field of view 2.34 mm.

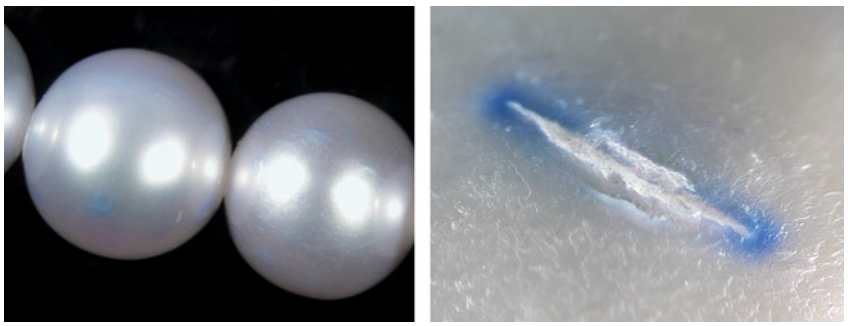

Figure 17. RTX image of freshwater BC pearls. The top strand, submitted for identification, has an average nacre thickness of 1 mm and an average bead diameter of 3.5 mm. The bottom strand, from the Hong Kong show, has an average nacre thickness of 0.8 mm and an average bead diameter of 2.7 mm.

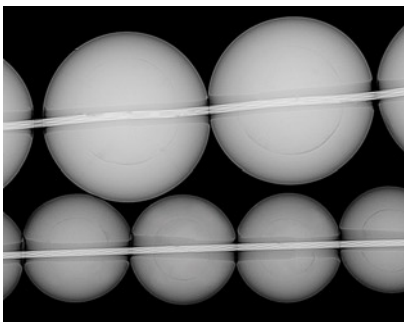

also very small akoya BC pearls below 3 mm in the market (Spring 2018 Gem News International, pp. 103–105). Due to the popularity of very small round BC pearls, the size range of these types of freshwater and akoya pearls can be very similar. It could be difficult to separate them through visual inspection, and more advanced methods are likely needed to verify the environmental origin. The slightly flat surface feature previously encountered on white freshwater BC pearls was not present on the samples studied here (Spring 2023 Gem News International, pp. 109–110). Moreover, our freshwater BC pearl samples showed thicker nacre compared with the very small akoya pearls previously reported, with a nacre that was above the usual commercially accepted range (0.15–0.50 mm) for akoya.

Chinese freshwater cultured pearls are widely available in various sizes, shapes, colors, and qualities and have become a major part of the global market. This was GIA's first examination of such small freshwater BC pearls, demonstrating the versatility of Chinese freshwater culturing methods in adapting to consumer demands.

Amiroh Steen, Joyce Wing Yan Ho, and Artitaya Homkrajae

Unusual Large Nacreous Pen Pearls

GIA's Mumbai laboratory has received a wide variety of interesting pearls for identification since opening its pearl testing department in May 2022. One recent submission included three baroque pearls weighing 24.47 ct, 36.58 ct, and 36.70 ct and measuring 28.22 × 18.04 × 9.84 mm, 28.79 × 19.48 × 10.40 mm, and 32.49 × 20.50 × 18.35 mm, respectively (figure 18).

Visual observation revealed a combination of nacreous and non-nacreous surface structures. The pearls were white to light gray and brown and exhibited a strong orient with variations in saturation and tone. In some areas, their surface quality was poor to slightly damaged. Viewed under 40× magnification, the white to light gray areas displayed a striated and much finer form of nacre growth structure than observed in most nacreous pearls from *Pinctada* and *Pteria* mollusks (figure 19, left). The dark brown areas showed a characteristic non-nacreous cellular structure consisting of a network of closely packed cells (figure 19, right). These observations were consistent with previous studies (N. Sturman et al., "Observations on pearls reportedly from the Pinnidae family (pen pearls)," Fall 2014 *G&G*, pp. 202–215).

Figure 18. Left to right: Three large nacreous pearls weighing 24.47 ct (pearl 1), 36.58 ct (pearl 2), and 36.70 ct (pearl 3).

Raman analysis using a 514 nm and 830 nm laser excitation was performed on different surface areas. The nacreous areas on all three pearls showed a doublet at 701 and 704 cm^{-1} and a peak at 1085 cm^{-1} indicative of aragonite. However, the brown non-nacreous areas on pearls 1 and 2 showed a peak at 712 cm^{-1} indicative of calcite. Photoluminescence analysis for all pearls revealed weak bands at 620, 650, and 680 nm, suggesting natural coloration (S. Karampelas et al., "Raman spectroscopy of natural and cultured pearls and pearl producing mollusc shells," *Journal of Raman Spectroscopy*, Vol. 51, No. 9, 2020, pp. 1–9).

Despite the possibility of these three being large blister pearls, closer examination of them did not reveal any indications of previous attach-

Figure 19. Features characteristic of pen pearls shown on pearl 1. Left: Striated nacre on the white and light gray areas; field of view 3 mm. Right: Non-nacreous structure consisting of a network of cells observed on the dark brown region; field of view 1.3 mm.

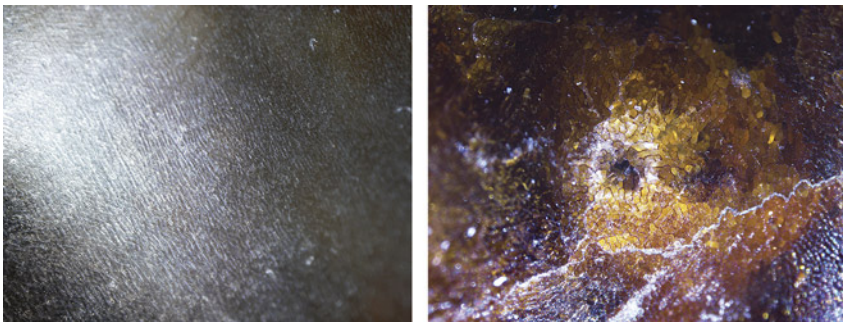

ment to the shell such as signs of heavily worked or sawn areas ("Natural shell blisters and blister pearls: What's the difference?" *GIA Research News*, August 26, 2019). The lack of such features indicated they were whole pearls. The few small organic-rich areas visible on the pearls' surfaces (figure 20), along with the non-nacreous and nacreous surfaces, were possibly damaged because the organic-rich material weakened over time.

X-ray fluorescence analysis revealed an inert reaction for all the samples. Energy-dispersive X-ray fluorescence spectrometry showed very low manganese levels (below detection limit in both pearls 1 and 2 and 9.9 ppm in pearl 3) and high strontium levels (1535 ppm, 1682 ppm, and 1250 ppm, respectively). Both analytical results were indicative of a saltwater origin.

Real-time microradiography (RTX) and X-ray computed microtomography (μ-CT) revealed a combination of large voids with some dark organic-rich material surrounded by white walls and fine growth arcs (figure 20). A chambered effect was notable in all three samples. The complex appearance of the voids differed from those observed in most non-bead cultured pearls from the *Pinctada* species, yet they were similar to nacreous and non-nacreous pen pearls reported in Sturman et al. (2014). The outline of the voids was consistent and followed the shape of the pearls' surfaces, unlike the irregular and inconsistent voids found in the non-bead cultured pearls. In addition, μ-CT imaging revealed light gray and dark gray areas associated with the presence of organic matter within the voids, a characteristic commonly observed in natural pearls ("Non-bead cultured pearls from *Pinctada margaritifera*," *GIA Research News*, April 27, 2018).

Based on the external and internal structure analysis, the samples were identified as natural pearls from the *Pinnidae* family (pen pearls). Visual observation, combined with the absence of any evidence of commercial culturing, played a crucial role in their identification. Their size and appearance further supported their classification as natural whole pearls.

Karan Rajguru, Abeer Al-Alawi, and Roxane Bhot Jain

Figure 20. RTX images, μ-CT images, and photomicrographs of the three pearls. The dark organic-rich voids are marked with red arrows, and the external weakened organic-rich areas on the surface are marked with blue arrows. Fields of view 9 mm (pearl 1) and 16.3 mm (pearls 2 and 3).

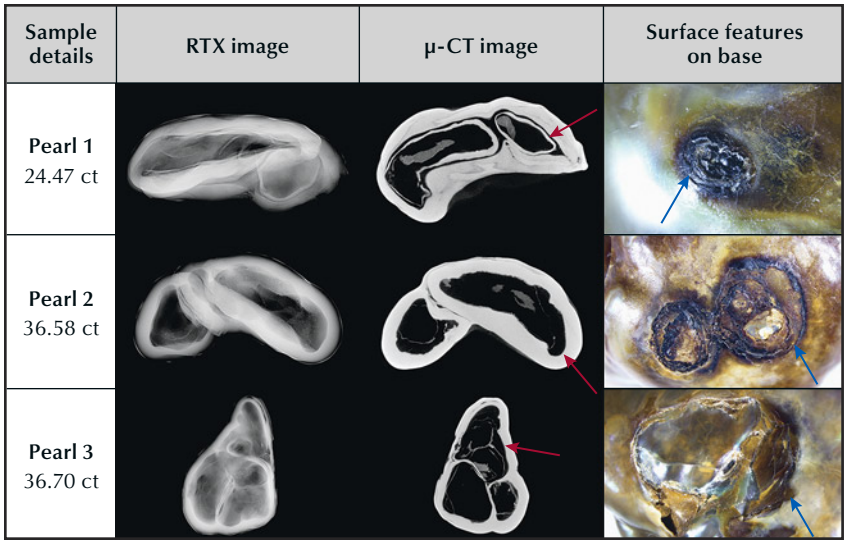

Seed Pearls in an Antique Indian-Style Headdress

Identification of seed pearls often poses a challenge to gemologists. Seed pearls are typically smaller than 3 mm and can be of either saltwater or freshwater origin (*The Pearl Blue Book*, CIBJO, 2022). These tiny pearls have long been used for adornment on clothing, jewelry, and various decorative items.

Recently, GIA's Mumbai laboratory examined an antique headdress (figure 21) submitted for pearl identification service. The exquisite headdress, which according to the client dates back several decades, featured intricate embroidery on a red velvet base. It incorporated approximately 7,000 light cream and cream-colored pearls, most of which displayed a strong orient. These pearls, ranging from semi-baroque to baroque in shape, were meticulously hand-woven onto the headdress using white silk thread and further secured by a surrounding framework of twisted white metal wire. The headdress itself weighed 240 g, and most of the pearls measured around 2.10 mm, with some larger ones reaching up to 3.40 mm.

Under a 10× loupe, some of the pearls displayed slight wear around the drill hole, while maintaining an overall intact nacre condition with a medium to high surface luster. The pearls embroidered on top of the headdress displayed nacreous overlapping aragonite platelets (platy structure) patterns, which are typically observed in pearls from a saltwater environment. Those on the side portion exhibited slightly broader platy patterns, which are common in freshwater pearls. Under long-wave ultraviolet radiation (figure 22, top), most of the pearl samples showed weak greenish yellow fluorescence, with a small percentage showing yellowish brown. A similar weaker reaction was observed under short-wave ultraviolet radiation (not shown).

When exposed to X-ray fluorescence, the pearls on top of the headdress were inert, indicating their

Figure 21. This antique Indian-style headdress is decorated with hand-woven light cream and cream-colored seed pearls.

saltwater origin. In contrast, the pearls on the side portion showed a strong yellowish green fluorescence due to high manganese contents, indicating a freshwater origin (figure 22, bottom). Interestingly, some freshwater pearls also displayed an orangy red fluorescence, suggesting the presence of vaterite, a less commonly observed form of calcium carbonate ($CaCO_3$) compared to aragonite or calcite (Winter 2021 Lab Notes, pp. 377–378). Due to the size and delicate nature of the headdress, further analysis of chemical composition using energy-dispersive X-ray fluorescence spectrometry was not feasible.

To study the internal structures, the authors performed random sampling using real-time microradiography (RTX) imaging (figure 23). Internally, most of the saltwater pearls exhibited small organic-rich cores with fine growth arcs, while other samples displayed tight to minimal structures with a few fine growth arcs toward the outer nacre. These internal structures were similar to those observed in natural pearls from the *Pinctada* species. Similarly, the freshwater pearls displayed natural structures with growth arcs throughout the pearl, consistent with natural freshwater pearls from GIA's research database (Summer 2021 Gem News International, pp. 167–171). Twisted linear structures or voids, which are commonly found in non-bead cultured Chinese freshwater pearls, were also observed in a minority of the tested samples (K. Scarratt et al., "Characteristics of nuclei in Chinese freshwater cultured pearls," Spring 2000 *G&G*, pp. 98–109).

Although the identification of seed pearls has always presented challenges and limitations, advancements in equipment and instrumentation available at GIA laboratories enable the detailed analysis of even the most minute structures and features in pearls, whether natural or cultured.

Roxane Bhot Jain, Jayesh Surve, Abeer Al-Alawi, and Chunhui Zhou

Figure 22. Top: Long-wave ultraviolet reaction displaying a greenish yellow reaction and an occasional yellowish brown reaction. Bottom: Freshwater pearls emitting a strong yellowish green XRF reaction; some orangy red fluorescence suggesting vaterite.

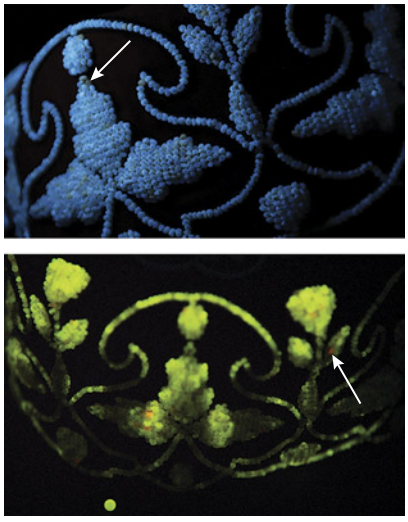

Figure 23. Left: RTX image of pearls from the top portion of the headdress (saltwater environment). Right: RTX image of pearls from the side portion (freshwater environment).

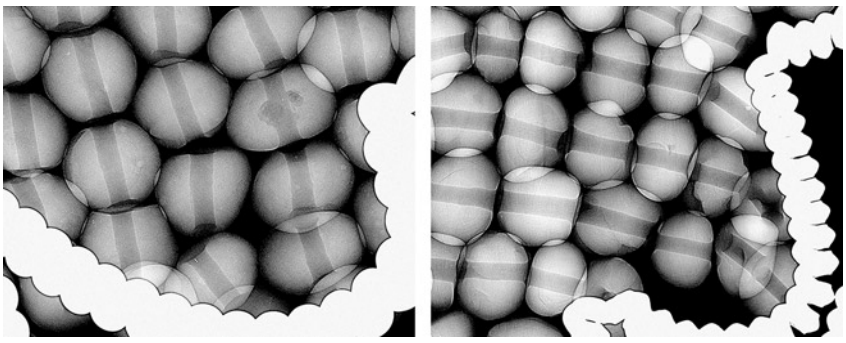

Figure 24. This 1.27 ct white semi-baroque pearl exhibited a typical platy structure when examined under magnification.

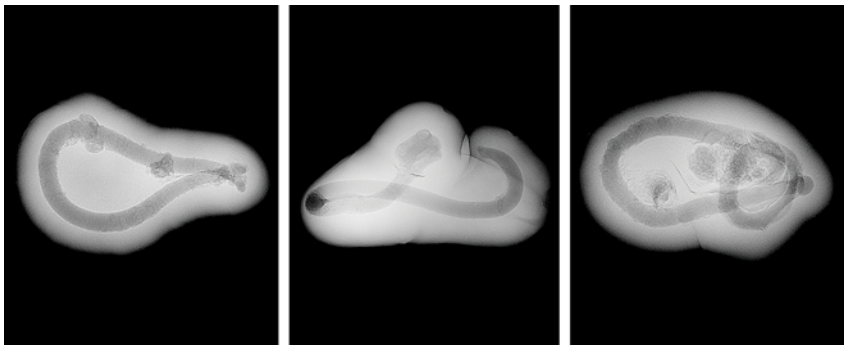

Figure 26. Similar tubular features observed in three reportedly natural saltwater pearls weighing 0.25, 0.34, and 0.44 ct, respectively, sourced from Pinctada radiata *mollusks from the waters of Bahrain.*

Tubular Feature in a Natural Pearl

Recently, GIA's Bangkok laboratory received a 1.27 ct white semi-baroque pearl for pearl identification service (figure 24). Under 40× magnification, the surface exhibited typical nacreous overlapping aragonite platelets (platy structure).

Real-time microradiography (RTX) revealed a tubular feature like a twisted tunnel at the center of the pearl, surrounded by fine growth arcs. When observed along the pearl's thickest direction, the feature resembled a void or cavity-like structure (figure 25, left), similar to those found in non-bead cultured pearls ("The microradiographic structures of non-bead cultured pearls," *GIA Research News*, November 20, 2009). However, when viewed from its flat direction (figure 25, center), the elongated tubular nature of the feature was inconsistent with the voids observed in non-bead cultured pearls. This inconsistency was further supported by X-ray computed microtomography (μ-CT), which showed multiple interconnected rounded voids (figure 25, right). When exposed to X-ray fluorescence, the pearl displayed an inert reaction indicative of a saltwater environment.

While this was the first time the lab had encountered a client submission with such a structure, similar structures were previously documented in three reference pearl samples from GIA's research database. The three were reported to be natural *Pinctada radiata* pearls sourced from the waters of Bahrain; they were baroque and weighed 0.25, 0.34, and 0.44 ct (figure 26). Those samples showed a similar elongated twisted tubular feature at their center in RTX and μ-CT scan imaging, which helped confirm the natural origin of the examined pearl.

To further study this tubular feature, three-dimensional models were created using specialized software to render the μ-CT scan images ("New 3-D software expands GIA's pearl identification capabilities," *GIA Research News*, May 13, 2016). The results from these models clearly showed that the central structure consisted of an elongated twisted tube. Based on the tubular formation presented, the feature is suspected to be formed by a burrowing parasite trapped in the center of the pearl (figure 27; see video of the 3D model at www.gia.edu/gems-gemology/winter-2023-lab-notes-tubular-feature-natural-pearl). Parasites of various types have been observed in both saltwater and freshwater bivalves, and certain worms have been known to use bivalve mollusks as their hosts. Notably, marine bivalve mollusks tend to be more prone to parasitic intrusions than freshwater mussels (E. Strack, *Pearls*, Rühle-Diebener-Verlag, Stuttgart, 2006, p. 116). Therefore, the presence of such tubular features in saltwater pearls indicates the potential

Figure 25. Left: RTX image taken along the pearl's thickest direction showing a stacked internal structure that could be misinterpreted as a void typically observed in non-bead cultured pearls. Center: RTX image from the flat direction revealing a tubular feature in the center. Right: μ-CT image revealing multiple interconnected rounded voids.

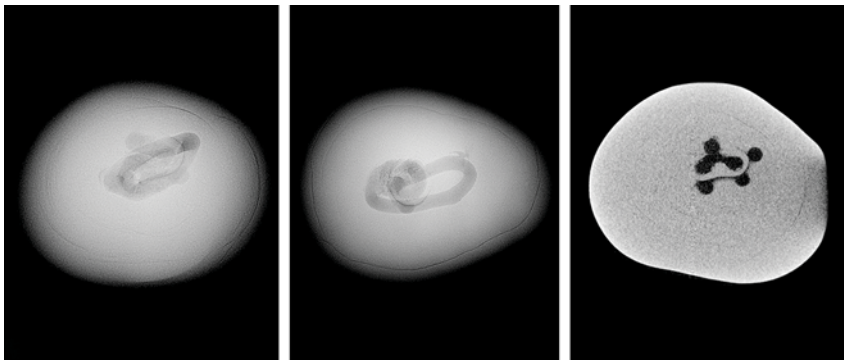

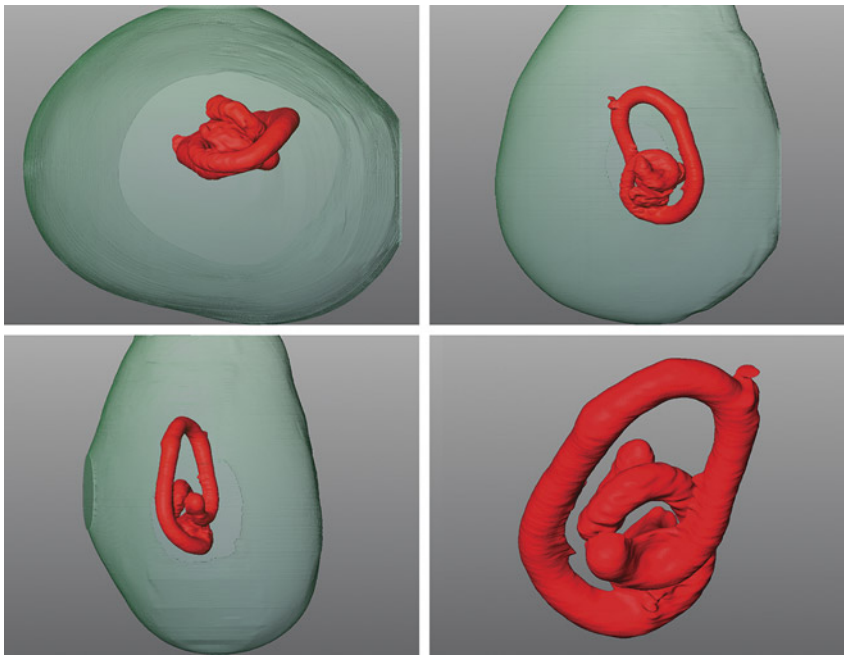

Figure 27. The 3D models generated using µ-CT scans revealed the tunnel-like feature (red) suspected of being parasite remnants or evidence of parasitic activity within the pearl.

infiltration of worm larvae into the mollusks' mantle. These larvae—either dead, alive, or hibernating—may have subsequently become encapsulated by the mantle epithelial cells, leading to the formation of a pearl sac and eventually the creation of a pearl.

Ravenya Atchalak and Emiko Yazawa

A Remarkable 16.71 ct Transparent Orange-Yellow SODALITE

GIA's Bangkok laboratory recently examined the 16.71 ct transparent orange-yellow faceted oval shown in figure 28. Standard gemological testing revealed the stone to be singly refractive with a refractive index of 1.484 and a hydrostatic specific gravity of 2.28. The stone showed strong orange fluorescence under long-wave ultraviolet light and weak orange with chalky white fluorescence under short-wave UV. Microscopic examination revealed internal features such as a fingerprint-like plane of two-phase fluid inclusions and numerous tiny transparent crystals. Raman spectroscopy analysis using 514 nm laser excitation showed several distinct peaks at 263, 294, 464, 969, 986, and 1058 cm^{-1}, which are characteristic features of sodalite (B. Lafuente et al., 2015, http://rruff.info/about/downloads/HMC1-30.pdf). Energy-dispersive X-ray fluorescence also identified the main chemical composition as sodium, aluminum, silicon, and chlorine, consistent with sodalite, which falls into the feldspathoid mineral group $Na_8(Al_6Si_6O_{24})Cl_2$.

Figure 28. A 16.71 ct transparent orange-yellow oval sodalite measuring 17.61 × 15.74 × 12.88 mm.

Sodalite is typically a semitransparent to opaque blue stone with calcite veining resembling lapis lazuli. However, it can occasionally exhibit other colors. The orange-yellow variety of sodalite is rare, and its color may be related to the presence of sulfide ions (F. Seel, "Sulfur in artwork: Lapis lazuli and ultramarine pigments," *Studies in Inorganic Chemistry*, Vol. 5, 1984, pp. 67–89). Ultraviolet/visible spectroscopy showed an absorption band centered at approximately 480 nm, likely caused by heavy radioactive elements creating an unstable color center substituting for Cl^- in a tetrahedron of Na^+ ions (H. Annerstein and A. Hassib, "Blue sodalite," *Canadian Mineralogist*, Vol. 17, 1979, pp. 39–46; P.S. Pizani et al., "Color centers in sodalite," *American Mineralogist*, Vol. 70, 1985, pp. 1186–1192). This sodalite is exceptional for its color, transparency, and 16.71 ct size. To the author's knowledge, this is GIA's first encounter with a large faceted orange-yellow sodalite.

Narint Jaisanit

Rare Faceted THOMSONITE

The Carlsbad laboratory recently examined a colorless semitransparent 1.04 ct oval modified brilliant (figure 29). Standard gemological testing gave a specific gravity (SG) of 2.47 and a refractive index of 1.520–1.538. These properties suggested the stone was a rare faceted thomsonite, which was confirmed by Raman spectroscopy. There are two types of thomsonite: the more common thomsonite-Ca with the chemical formula $NaCa_2Al_5Si_5O_{20} \cdot 6(H_2O)$ and the less common thomsonite-Sr with the chemical formula of $Sr_{1.4}Ca_{0.6}NaAl_5Si_5O_{20} \cdot 7.1(H_2O)$. X-ray fluorescence was not run on this stone to determine which, for fear of damag-

Figure 29. A rare 1.04 ct semitransparent thomsonite measuring 7.53 × 6.15 × 4.67 mm. The inset shows the typical appearance of thomsonite.

ing the potentially fragile stone. The SG reading was slightly higher than the expected value of 2.35 (+0.05/–0.10). Multiple surface scratches and abrasions indicated a relatively soft material, consistent with thomsonite's hardness of 5.0–5.5 on the Mohs scale. This specimen featured a radiating fibrous inclusion resembling a snowflake (figure 30). Although the identity of the inclusion could not be confirmed with Raman spectroscopy, it was likely a member of the zeolite group.

Thomsonite is a rare member of the zeolite group named for Scottish chemist and mineralogist Thomas Thomson (1773–1852). While the source of this specimen is unknown, thomsonite is typically found in Minnesota along Lake Superior. It usually occurs as semitranslucent to opaque rounded crystal aggregates (figure 29, inset) with a fibrous structure. Thomsonite has also been known to appear as part of a rock aggregate (B.M. Laurs et al., "Benitoite from the New Idria District, San Benito, County, California," Fall 1997 *G&G*, figure 13) or as rare needle inclusions in Canadian sapphires (Winter 2004 Gem News International, pp. 344–345). Semitransparent and faceted thomsonite is very unusual. To the best of our knowledge, this is the first faceted thomsonite examined by GIA.

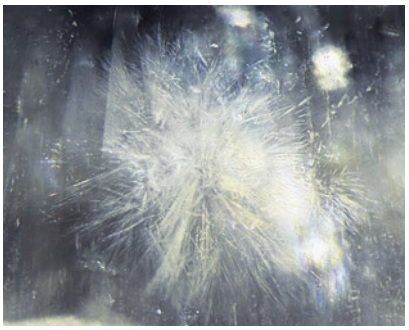

Figure 30. A fibrous snowflake-like inclusion found within the semitransparent thomsonite. Field of view 3.57 mm.

Michaela Damba

PHOTO CREDITS
Adriana Robinson—1, 15, 29; Stephanie Shaw—2; Mei Yan Lai—3–5; Priyanka Kadam—6; Diego Sanchez—8; Nathan Renfro—9; Tony Leung—12; Artitaya Homkrajae—16; Joyce Wing Yan Ho—17; Gaurav Bera—18, 21; Karan Rajguru—19, 20; Lhapsin Nillapat—24, 28; Scott Lewis—29 (inset); Michaela Damba—30